Journal of Environment and Sustainable Mining Vol.1 No.3 (2025) 49-68

Journal of Environment and Sustainable Mining

University of Sistan and Baluchestan

Iranian Society of Mining Engineering (IRSME)

Petrography and geochemistry of mafic to acidic dikes in Siahjakuk, south of Zahedan, southeastern Iran

Mohammad Bameri[1]*, Habib Biabangard[1], Parvaneh Bijar[1]

[1]Geology Department, University of Sistan and Baluchestan, Zahedan, Iran.

ARTICLE INFO

Article type:
Research Article

Article history:
Received: 2025-07-21
Received in revised form: 2025-08-28
Accepted: 2025-09-22
Published online: 2025-09-29

Keywords:
Conjugate dikes,
Whole rock chemistry,
High-K calc-alkaline,
Post-collisional,
Sistan suture zone.

ABSTRACT

Siahjakuk dikes are located in the southeast and south of Zahedan in the Sistan Suture Zone. In this area, Eocene flysch-like rocks were intruded by numerous Oligocene dikes and some small stocks. The flysch is also intruded by Oligocene granitoid as a batholith in the southern part of the area. The flysch is mainly and locally altered phyllite, shale, sandstone, and siltstone. The dikes and flysch layers are mainly NW in strike, and there are also dikes with N-S and NE trends. Some dikes occur as conjugate dikes. The dikes sharply follow the faults and shear structures. The dikes are leucocratic to melanocratic in color and mafic to felsic in composition. They are meladiorite, diorite, granodiorite, granodiorite porphyry, diorite porphyry (andesite), dacite, and rhyolite. The dikes are mainly high K calc-alkaline, shoshonitic, and metaluminous and probably belong to post-collision magmatic arcs. The minor and rare earth elements, which are normalized to the primitive mantle and the chondrite, respectively, show that LREE and LILE are enriched over LREE and HESE, respectively, which is a feature of subduction-related igneous rocks in volcanic arcs. Concerning geochemical studies, the Siahjakuk dikes could assume an enriched, heterogeneous, and metasomatized lithospheric source. The mafic and intermediate dikes were formed from melts that derived from partial melting of mafic rocks such as basalt and amphibolite, and the acidic dikes are related to melts that derived from partial melting of crust sediments such as greywacke.

Cite this article: Bameri, M., Biabangard, H. and Bijar, P. (2025). Petrography and Geochemistry of Mafic to Acidic Dikes in Siahjakuk, South of Zahedan, Southeastern Iran. *Journal of Environment and Sustainable Mining*, 1(3), 49-68. https//doi.org/10.22111/jesm.2025.50428.1021

Publisher: University of Sistan and Baluchestan.
DOI: https//doi.org/10.22111/jesm.2025.50428.1021

* Corresponding author: **Mohammad Bameri**
E-mail address: mboomeri42@yahoo.com

1 .Introduction

The Siahjakuk is located in the south and southeast of Zahedan in the Sistan suture zone (SSZ) (Fig. 1). The SSZ is characterized by several igneous rocks and magmatic phases. The oldest igneous rocks in this zone are Cretaceous ultramafic to felsic rocks related to ophiolites. The younger magmatic rocks in this zone are magmatic phases related to post-collision magmatism due to the movement of Lut and Afghan blocks toward the SSZ. The study dikes are the last magmatic phase of this event. The study of dikes is important to interpret magma evolution and to know about magma nature and type of tectonic setting. Several studies have been carried out on the igneous rocks, including dikes in the Sistan Suture Zone [1, 2; 3; 4, 5, 6, 7, 8, 9]. This paper is the first work to investigate the petrography, geochemistry, and petrogenesis of these dikes and to provide new insight into the geodynamics of the area.

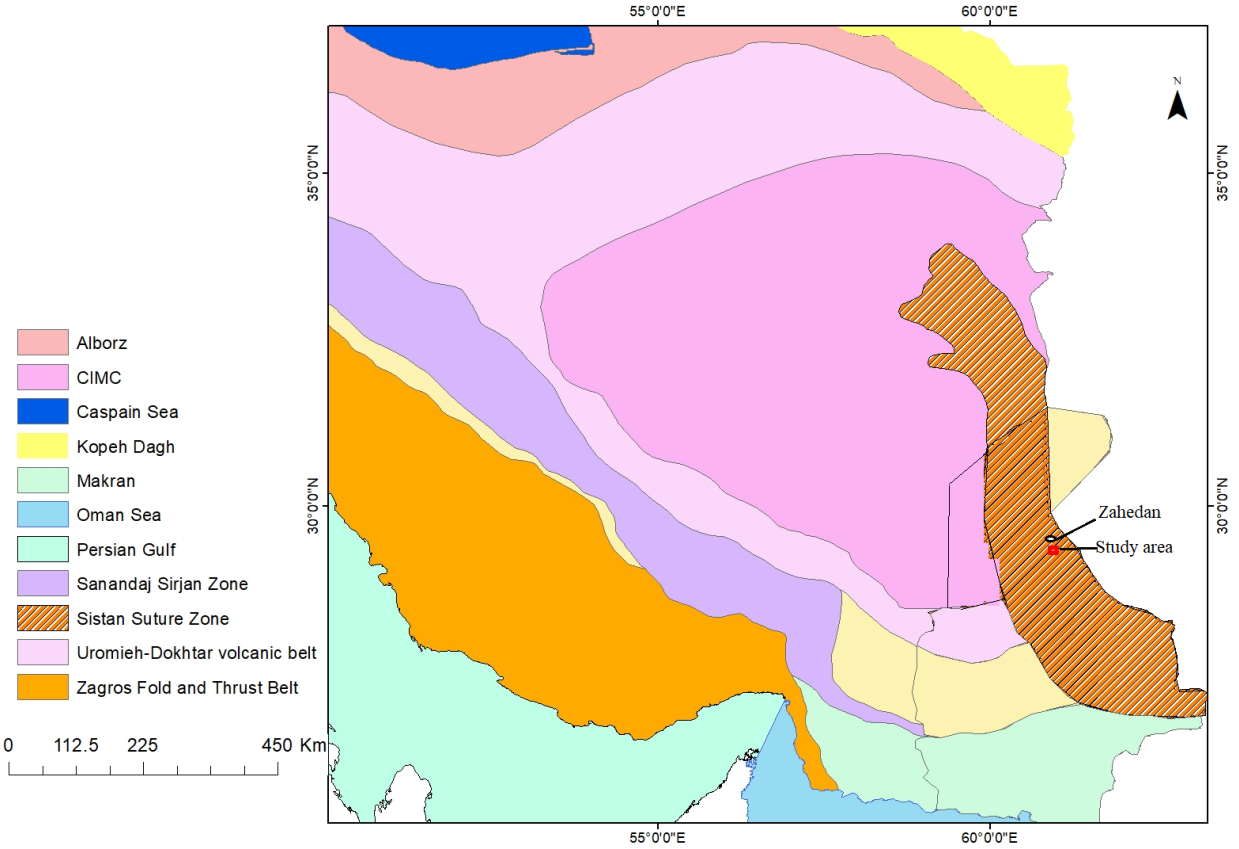

Fig. 1. Geological zones of Iran (SSZ) [modified from 10]. Legend is not in terms of age order. A black thin line that cuts some of the zones is the boundary of the Sistan and Baluchestan province.

1. Geology

2.1. Geology of the SSZ

The SSZ is a part of eastern and south-eastern Iran bounded by the Lut block from the west and the Afghan block from the east (Fig. 1) [10]. The geology of SSZ has been described in a few papers [1, 2]. According to these studies, the oldest rocks in the SSZ are Cretaceous ophiolites that are widespread throughout the SSZ, and the most abundant rocks are the Upper Cretaceous to Eocene turbiditic and flysch-like sedimentary rocks. The flysch-like rocks, including turbidites, originally are shale, sandstone, siltstone, limestone, marl, and conglomerate. The sedimentary rocks underwent weak metamorphism and were usually intruded and extruded by intermediate to acidic igneous rocks such as batholith, stock, dike, lava,

and pyroclastic from Cretaceous to Quaternary, giving rise to contact metamorphism and extensive alteration and mineralization [11, 12, 13, 14, 8, 9].

The metamorphic rocks in this zone are mainly schist, phyllite, slate, and hornfels. Development of the SSZ from the Middle Cretaceous has been affected by a series of important but short-term tectonic events [1]. During the Cretaceous, rifting separated the Lut and Afghan blocks and developed an ocean basin filled with flysch-like sediments. The Late Cretaceous-to-Eocene calc-alkaline rocks of SSZ, such as Nakhilab and Rudeshur igneous rocks and some parts of the Zahedan granitoid, were probably formed during subduction of the oceanic crust [3, 15, 7]. This event was followed by the collision of the Lut and Afghan blocks during Mid-to-Late Eocene, which was accompanied by the formation of the Zahedan batholith (Fig. 2). Oligocene to Middle Miocene and Pliocene post-collisional alkaline and calc-alkaline igneous rocks (shoshonite) occur as stocks, dikes, lava flows, and pyroclastic rocks in several parts of SSZ [1, 8]. Finally, the youngest rocks in the SSZ are Quaternary volcanic rocks (Mount Taftan) related to the active subduction of the Arabic plate under the Makran accretionary prism [16]. The alkaline and high-K calc-alkaline (shoshonitic) magmatism is closely related to major transcurrent faults. The strike-slip faults are important post-collisional structures of the SSZ [1, 17].

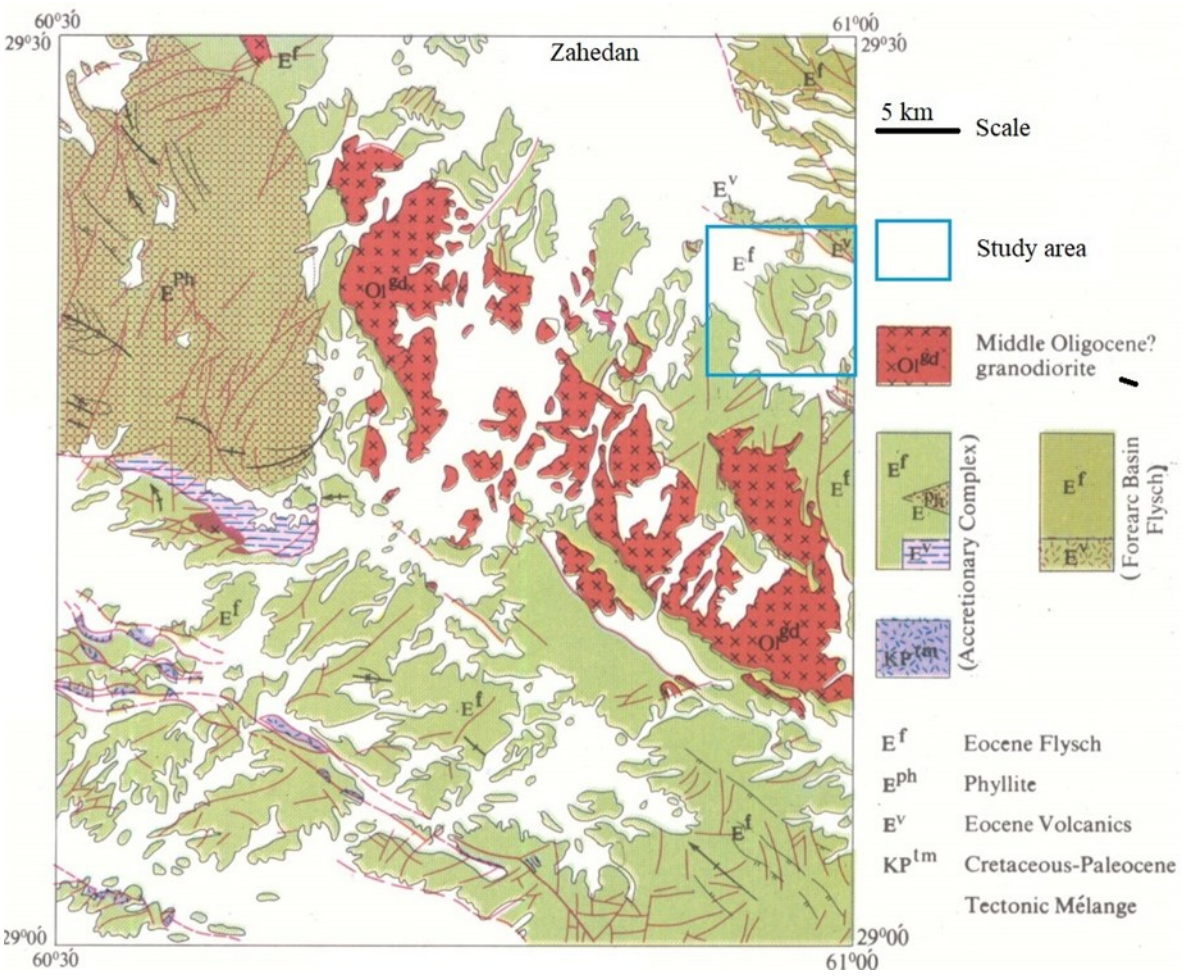

Fig. 2. A simplified geological Map of Zahedan and the location of the study area on it [17].

2.2. Geology of the study area

The sedimentary rocks, such as shale, fine-grained sandstone, and siltstone (flysch-like rocks), are the oldest (Eocene) and the most abundant rocks in the study area [18] (Figs. 2, 3 and 4). This unit is locally metamorphosed into slate and phyllite and altered to clay minerals. They are folded and schistose in structure and texture, and black, gray, green, brown, and cream in color. The general trend of the sedimentary rocks is NW-SE and locally W-E., and shows varied dips. This unit is intruded by Zahedan granitoids in the south of the study area (Fig. 2). The granitoids are mainly I-type and locally S-type, which have a general trend of SW-NE for more than 200 km in the northern part and NE-SW for more than 50 km in the southern part. The general trend of the granitoid is similar to the trend of the sedimentary rocks everywhere. The granitoid width is varied, but the average may be about 12 km in thickness. The granitoid occurs as a large batholith associated with stocks, dikes, and sills. They are mainly granodiorite associated with granite, tonalite, quartz monzonite, alkaline granite, and granular in texture [19]. The granitoids are mainly metaluminous, weakly metaluminous, and peraluminous and high-K calc-alkaline, similar to those that occur in the subduction-related tectonic settings [19].

The peraluminous granitoid in the SSZ occurs in sheared zones where they are severely faulted, locally brecciated, silicified, and mylonitized. They also show arc-like geochemistry characteristics with enrichment of LREE and LILE relative to HREE and HFSE, respectively, on chondrite and primitive mantle normalized spider diagrams [19].

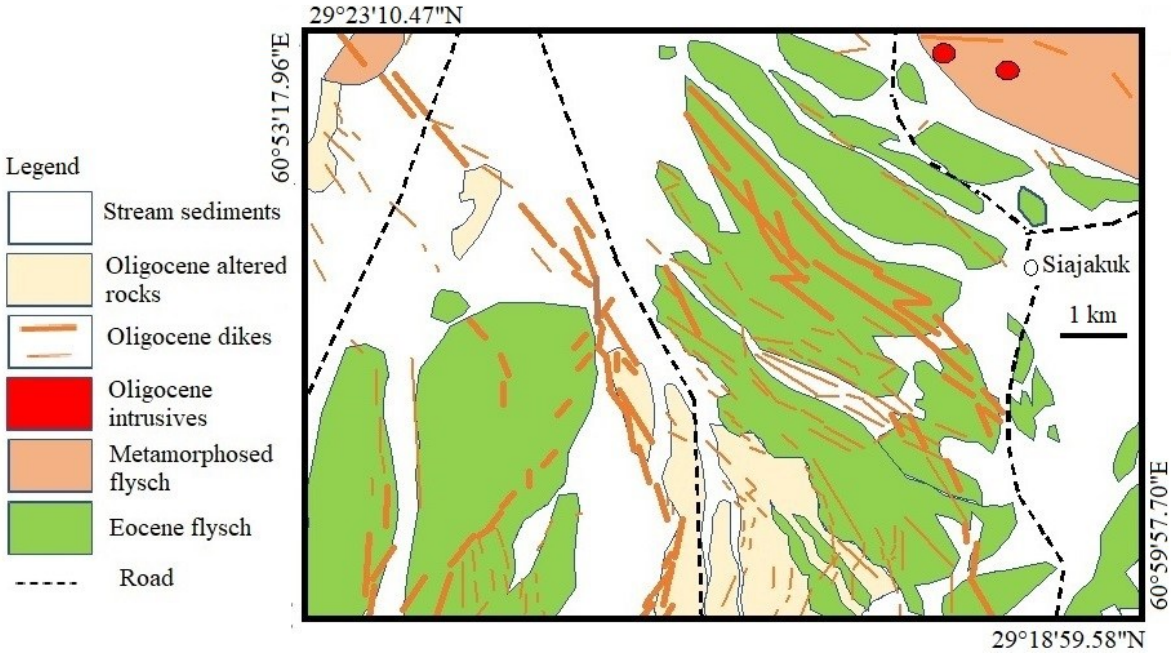

Fig. 3. A simple geological map of the Siahjakuk area.

Subvolcanic stocks are another unit in the study area with small outcrops (Fig. 4). This unit is weakly mineralized and composed of altered dacites, granodiorite, and granodiorite porphyry.

The dikes and sills are the youngest igneous phase in the study area that intruded the flysch-like sedimentary and metamorphic rocks, the granitoids, and the subvolcanic stocks. The dikes mainly occur as parallel or subparallel to layers and schistosity of the flysch-like rocks and appear mainly as a sill (Fig. 3). However, they cut across the host rocks in many localities. Conjugated dikes are common in the area, especially in the south of the study area. The general trend of the dikes in the study area is NW-SW and sometimes EW and NS. The dikes are usually long (up to several km) and have a small offset in width (Fig.

2). They are varied in thickness (from 3 to several meters) and color (black to white). The dikes and their host rocks show similar folding in some localities (Fig. 4). Some dikes are altered and contain pyrite crystals. A few mineralized quartz veins occur near altered dikes and contain abundant pyrite. All geological units have a faulted contact. The large movement of the geological units has been caused by NW and N-S faults, and small movements have been caused by NE faults.

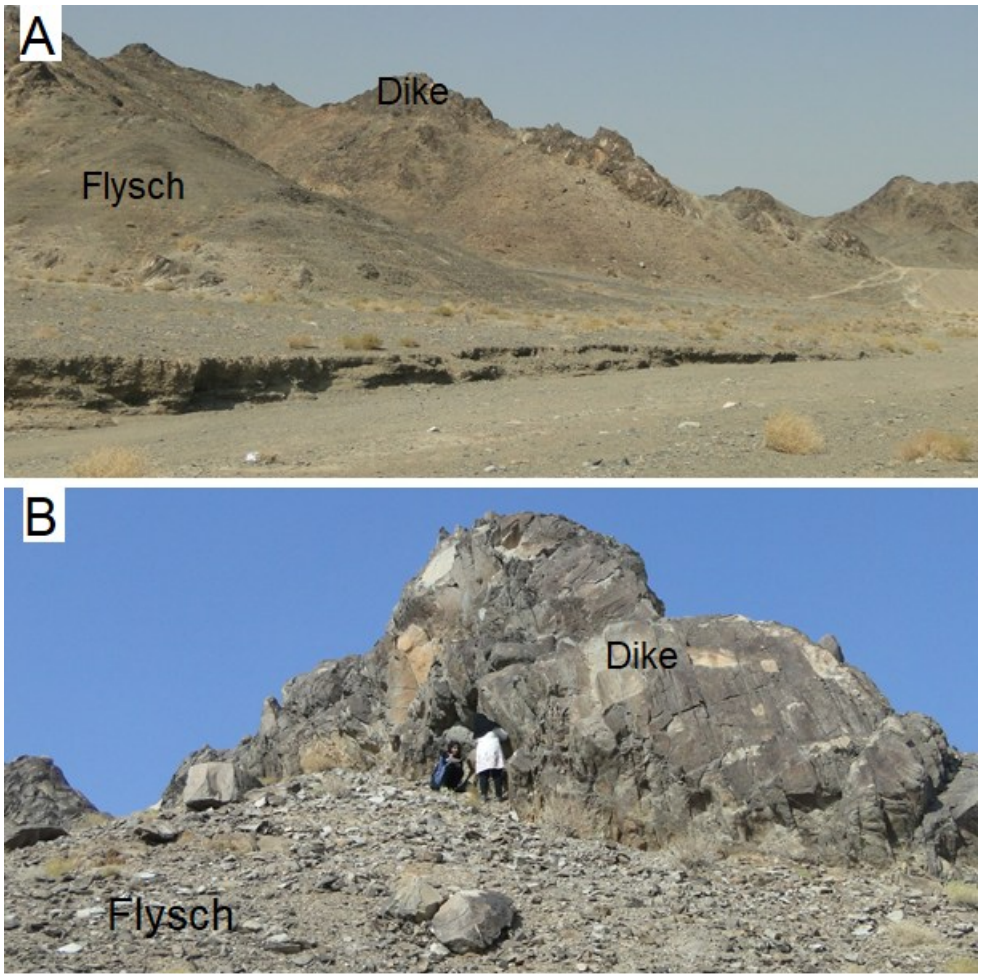

Fig. 4. (A) and (B) Field photographs of the flysch unit that was intruded by dikes in Siahjakuk.

2.2. Age of the igneous rocks

According to K/Ar dating [1] on biotite, the Zahedan granitoids range from 31 to 33 ± 2 Ma in age, while based on the U–Pb dating [7], their age ranges from 40.5 to 44.3 Ma. The igneous rocks in the north and northeast of Zahedan are Kuh-e-Lar, Kuh-e-Malek Siah, and Hormak basalts. According to K/Ar dating on the biotite grains, the age of the Kuh-e-Lar is 27.8 ± 3 Ma, while according to K/Ar dating of the whole rocks, the age ranges from 32 to 32.8 ± 3 Ma. According to K/Ar dating on amphibole, the age of the Kuh-e-Malek Siah ranges from 27.2 to 28.8 ± 4 Ma. Based on K/Ar dating of the whole rocks, the Hormak basalts are 27.0 ± 1.9 Ma in age [1]. These data show that Zahedan granitoids and Hormak basalts are the oldest and youngest igneous rocks, respectively, that intruded or extruded in the flysch-type rocks. Re-Os dating of two molybdenite samples from mineralized veins in monzonite and syenite yields ages of 29.72 ± 0.11 and 31.95 ± 0.11 Ma [8]. U-Pb dating of intermediate and felsic dikes that intruded the Zaheden

graniteoid yields ages of 28.95± 0.11 and 28.11± 0.65 m.y. [20]. This study shows that the Zahedan granitoid is 29.9 ± 0.1. The Siahjakuk dikes have similar or younger ages than these dikes.

3. Study method

A total of 40 samples were collected from different rock types, mainly from the dikes. 33 thin sections of these samples were prepared and studied by a polarized microscope at the University of Sistan and Baluchestan in Iran. Representative samples (15 samples) were then selected to analyze for major, minor, and rare earth elements of whole rocks. The Major elements were determined by the X-ray fluorescence (XRF) technique, and trace and rare earth elements were measured by ICP-MS techniques in Iran's high-tech laboratory network.

4. Petrography

The Siahjakuk dikes display different textures, mineralogy, and modal composition. Based on the petrography studies, the dikes are meladiorite, diorite, granodiorite, granodiorite porphyry, diorite porphyry (andesite), dacite, rhyodacite, and rhyolite (Figure 5E, F, G, H, and I).

4.1. Meladiorite

These dikes mainly occur in the east of the study area within metamorphosed flysch or phyllite and are usually less than 5 meters in thickness. The meladiorites are granular in texture and contain plagioclase, K-feldspar, quartz, hornblende, and biotite as primary minerals and chlorite, calcite, sericite, and clay minerals as secondary minerals (Fig. 5A and B). The amphibole is more than 30 % of the primary minerals of this rock type, which is locally associated with chloritized biotite. The mineral size shows a wide range, usually less than 2 mm in size (Fig. 5A and B). The amphiboles are mainly long and subhedral in shape and are partially altered to chlorite. The plagioclase, as the most abundant mineral, is mainly long, subhedral varies in shape, and is partially altered to sericite and clay minerals. The K-feldspar and quartz crystals are small and euhedral and occur among open spaces between other minerals. Calcite, as a secondary mineral, mainly occurs as open-space fillings.

4.2. Granodiorite

The granodiorite occurs as small stocks in the northeast of the study area and is granular in texture and consists of quartz (30 %), plagioclase (35 %), and minor K-feldspar, biotite, hornblende, opaque minerals, and secondary minerals (Figure 5C). The minerals of this rock are the largest in size relative to other study rock types in the study area. The crystals are rarely larger than 2 mm in size. Quartz occurs as medium-sized grains clustered between other minerals. Some of the quartz grains are secondary and were formed by alteration processes. The plagioclase occurs as subhedral grains and is characterized by polysynthetic twining and zoning, and is subject to sericitic and propylitic alteration types. Amphibole and biotite are mainly altered to chlorite and epidote. The propylitic alteration is intensive in this rock, which is characterized by epidote, chlorite, calcite, quartz, and pyrite. This rock hosts weak Cu mineralization, including Cu carbonates.

4.3. Diorite

The diorite has a similar mineralogy and texture to meladiorite. The difference is the lower volume percent of ferromagnesian minerals in the diorite, which are less than 30 % of the primary minerals. The most abundant mineral is plagioclase (more than 50 %), which is characterized by polysynthetic twining and small crystals (Fig. 5D). It shows variable sericitization and calcification, shape, and size. The hornblende and biotite occur as long subhedral-colored crystals with variable alteration to chlorite and epidote. Quartz and K-feldspar optical characteristics are similar to those in the meladiorite. Calcite occurs as open space filling, microveinlet, and replacement.

4.4. Granodiorite porphyry

Granodiorite porphyry occurs as a dike and stock in the western part of the area and has a porphyry texture. The groundmass is about 30 % of the rock and mainly consists of anhedral crystals of feldspar and quartz, and secondary minerals such as phyllosilicates. The main phenocryst is plagioclase associated with quartz, orthoclase, and biotite. Some samples are affected by potassic alteration that is characterized by hydrothermal biotite and orthoclase (Fig. 5E).

4.5. Andesite (diorite porphyry)

These dikes have a porphyry texture composed of a groundmass and a few phenocrysts (Figure 5F). The groundmass is totally crystalline and composed mainly of plagioclase and quartz grains with variable sizes. The phenocrysts are mainly plagioclase (more than 80% of primary phenocrysts), hornblende, biotite, and little quartz (Fig. 5F). The plagioclase crystals usually display well-developed zoning and twinning. They are variable in size and shape and show variable alteration to sericite. Biotite is less or more replaced by chlorite, and amphibole crystals are sometimes opacitized and altered, and have dark rims rich in Fe and Ti oxides. The secondary minerals are chlorite, quartz, calcite, clay minerals, and epidote. Opaque minerals are mainly pyrite and magnetite.

4.6. Dacite and rhyolite

The dacite and rhyolite occur as white dikes and small stocks in the area and have a different color (white) in outcrops relative to other study dikes. They are less abundant than intermediate and basic dikes. The Dacite and rhyolite are porphyry in texture and consist of plagioclase, quartz, and sanidine (Figure 5G, H, and I).

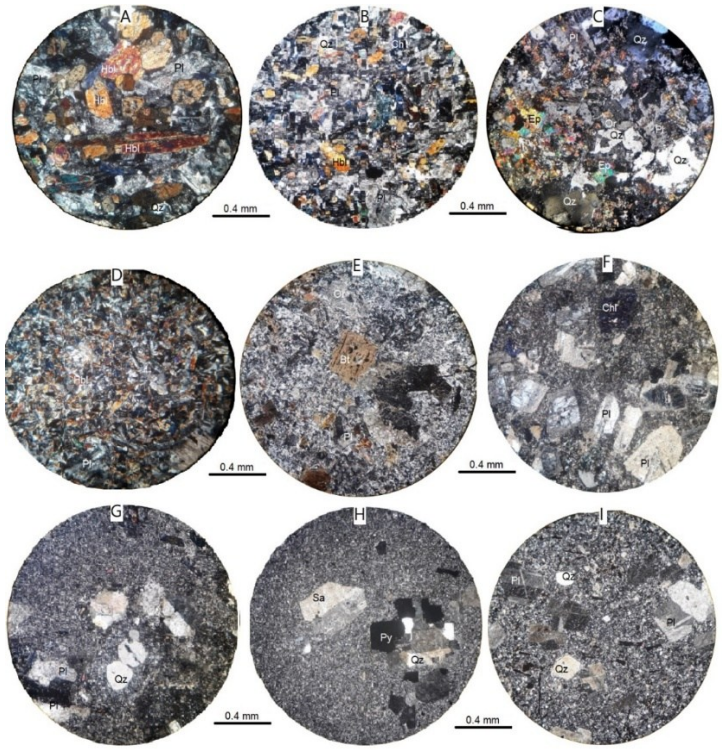

Fig. 5. Microphotographs of the rock types in the Siahjakuk. (A) meladiorite, (B) meladiorite, (C) granodiorite, (D) diorite (E) granodiorite porphyry (F) andesite (diorite porphyry) (G) dacite (H) rhyodacite (I) dacite. Qz=quartz, Pl=plagioclase, Hbl=hornblende, Bt=biotite, Chl=chlorite, Or=orthoclase, Sa=sanidine, Py=pyrite. Abbreviations from Whitney and Evans [20].

The groundmass volume ranges from 50 to 80 % of the rocks in the study samples and is composed of fine-grained crystals of quartz that are associated with little feldspar and secondary phyllosilicates. The phenocrysts are mainly less than one mm in size. The plagioclase phenocrysts are subhedral to euhedral, twinned and zoned, and partially altered to sericite. The sanidine is euhedral to subhedral in shape and has a carlsbad twin. The biotite and amphibole are rare in the dacitic and rhyodacitic dikes. These dikes had been affected by phyllic alteration and sericite, quartz, orthoclase, calcite, pyrite, and clay minerals in which occur as microveinlets, replacements, and other space-filling textures.

5. Geochemistry

The major, minor, and RE elements analyses are reported in Table 1. These elements have been used to describe the geochemical characteristics of the study rocks and related magmas as follows:

Table 1. Major and trace elements of dikes in Siahjakuk in terms of wt. % and PPM, respectively.

Sample	S35	S18	S34	S21	S33	S3	S8	S14	S31	S44	S22	S39	S28	S11	S12
Rock	meladiorite						diorite		granodiorite			dacite		rhyolite	
SiO_2	46.5	48.3	50.6	51.0	51.0	52.6	55.0	56.9	60.9	61.2	61.4	64.3	66.9	71.6	72.1
TiO_2	1.43	1.37	1.46	1.33	1.06	1.53	1.19	0.76	0.85	0.55	0.90	0.66	0.42	0.50	0.50
AI_2O_3	14.6	14.3	16.8	14.2	14.4	15.2	14.9	15.0	14.7	14.1	14.5	15.5	15.1	15.5	14.5
Fe_2O_3	11.1	10.5	9.82	7.21	9.50	8.49	7.73	7.07	5.48	6.91	5.53	4.71	2.87	0.84	0.94
CaO	9.39	8.22	6.94	5.67	7.59	6.74	5.94	3.13	4.52	5.14	4.22	3.70	2.00	0.57	1.05
MgO	7.67	8.21	3.92	6.42	8.17	5.86	5.44	6.90	2.40	4.13	3.96	1.34	0.90	0.31	0.10
K_2O	2.11	2.06	2.53	3.10	1.98	2.56	2.61	1.96	3.75	0.32	3.38	3.73	4.59	5.25	5.20
Na_2O	2.86	3.24	3.55	2.85	2.74	3.48	3.82	3.05	3.30	4.64	3.59	3.83	3.93	4.27	3.41
P_2O_5	0.30	0.31	0.20	0.22	0.18	0.29	0.19	0.13	0.14	0.10	0.16	0.16	0.15	0.15	0.15
L.O.I	3.6	3.1	3.8	7.6	2.9	2.9	2.9	4.7	3.7	2.4	2.1	1.8	3.1	1.3	2.1
Total	99.5	99.6	99.6	99.6	99.6	99.7	99.6	99.6	99.8	99.5	99.8	99.7	100	100	100
Ba	350	485	370	1172	421	334	325	408	500	460	509	478	463	608	590
Co	29.5	32.5	23.3	27.5	32.4	32.9	22.8	30.1	16.2	9.9	16.2	10.2	3.6	1.0	1.0
Cr	58	373	28	202	432	220	249	299	88	45	171	55.7	65.4	43.6	43.4
Cu	30.0	72.0	44.6	70.2	55.3	48.6	49.1	63.2	49.1	39.9	49.4	39.3	35.5	32.6	31.7
Hf	1.6	1.7	1.5	1.7	2.2	1.4	1.8	1.6	1.5	1.2	1.3	1.4	0.5	1.0	0.7
La	18.1	19.5	14.4	25.3	13.8	21.9	17.4	14.3	13.7	8.2	14.6	11.0	6.5	2.7	2.6
Ce	36.3	36.8	28.1	46.8	27.9	42.7	33.6	27.2	26.9	16.4	28.1	22.4	13.1	5.7	5.6
Pr	3.9	3.9	3.1	4.6	3.0	4.6	3.5	3.0	2.9	1.8	2.9	2.3	1.4	0.6	0.6
Nd	15.8	14.2	13.0	17.3	12.1	17.3	13.2	11.3	10.4	7.3	10.2	8.9	4.7	2.3	2.1
Sm	3.2	3.0	2.7	3.1	2.9	3.4	2.9	2.2	2.1	1.6	2.2	1.9	0.9	0.6	0.5
Eu	0.9	0.9	0.8	1.0	1.1	1.1	0.8	0.6	0.6	0.5	0.6	0.5	0.3	0.2	0.2
Gd	3.3	3.3	3.1	3.4	3.1	3.3	3.0	2.5	2.2	2.2	2.2	1.8	0.8	0.6	0.6
Tb	0.5	0.4	0.4	0.4	0.6	0.4	0.4	0.3	0.3	0.3	0.3	0.2	0.1	0.1	0.1
Dy	2.4	2.3	2.3	2.0	2.3	2.0	2.1	1.9	1.8	1.8	1.5	1.3	0.4	0.5	0.4
Ho	0.4	0.5	0.4	0.4	0.6	0.4	0.4	0.4	0.3	0.4	0.3	0.2	0.1	0.1	0.1
Er	1.3	1.3	1.2	1.0	1.4	1.0	1.1	1.0	0.9	1.1	0.8	0.6	0.2	0.3	0.2
Yb	1.0	1.2	1.0	1.0	1.0	1.0	1.0	1.1	0.9	0.7	0.8	0.4	0.2	0.2	0.2
Lu	0.1	0.2	0.1	0.1	0.1	0.1	0.1	0.1	0.1	0.1	0.1	0.1	0.0	0.0	0.0
Li	10.5	13.5	26.5	51.2	12.9	21.5	16.1	53.0	64.3	4.1	24.3	69.7	3.8	9.1	23.1

Nb	10.5	13.0	10.9	16.1	10.8	23.0	14.5	10.6	12.8	3.4	14.4	17.1	5.3	10.6	10.3
Ni	27	140	22	120	153	90	90	141	41	18	74	19	21	18	17
Pb	1.0	1.0	2.0	18.2	1.9	1.0	1.2	28.4	19.4	1.0	11.0	20.3	14.6	4.6	3.8
Rb	18.4	24.8	33.8	31.4	24.4	25.7	42.8	36.7	44.7	70.0	46.0	40.4	49.0	126	100
Sc	14.6	15.8	10.9	14.0	15.2	10.6	12.5	15.3	8.0	8.8	8.1	4.6	2.5	1.8	0.9
Sr	565	565	494	460	450	601	459	311	329	433	411	361	261	167	263
Ta	0.4	0.6	0.5	0.7	0.5	1.2	0.7	0.5	0.7	0.1	0.8	0.9	0.2	0.7	0.7
Th	1.7	1.9	2.1	5.6	4.7	1.8	3.3	4.3	6.4	1.0	6.2	4.4	3.6	3.3	2.4
V	41.7	162	136	161	160	104	125	104	78.2	136	81.7	48.3	43.2	16.7	15.3
Y	11.0	12.0	11.1	10.8	10.8	8.3	10.5	8.3	7.4	8.8	6.6	4.9	1.6	1.9	1.9
Zn	1.3	64.5	76.5	249	62.5	478	55.4	478	57.3	55.1	54.6	50.9	39.1	194	3.9
Zr	35.5	114	90.4	144	110	87.2	128	87.2	94.1	46.4	104	97.3	57.0	56.7	55.2

5.1. Chemical classification

There are several schemes and diagrams to divide igneous rocks based on chemical analyses. Some of them are for plutonic rocks, some of them are for volcanic rocks, and three are not an independent classification for subvolcanic rocks, such as dikes. Most researchers divide dikes similar to volcanic rocks. Here, the study samples are divided based on both extrusive and intrusive rocks chemical classification (Fig. 6). According to the SiO_2-(Na_2O+K_2O) diagram [22], the study dikes range from basic to acidic. This diagram also shows the rocks are chemically subalkaline and alkaline basalt and subalkaline andesite, dacite, and rhyolite (Fig. 6A) or alkaline gabbro and subalkaline gabbro, diorite, granodiorite, and granite (Fig 6B).

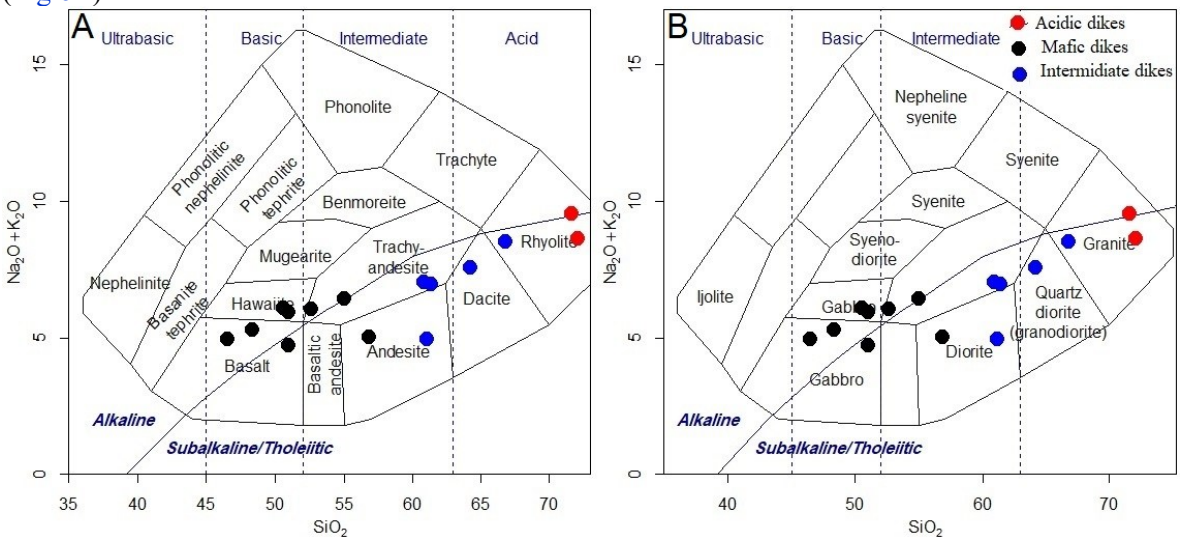

Fig. 6. Geochemical plots of the Siahjakuk dikes in the total alkali vs. silica classification diagram. (A) extrusive rocks (b) intrusive rocks.

5.2. Major elements

SiO_2 contents of the dikes show a wide range from 72 to 46.5 wt%. Major element variations versus SiO_2 are illustrated in Harker binary diagrams [23] (Fig. 7). The TiO_2, CaO, Fe oxides, and MgO contents decrease as SiO_2 increases, and they display a negative correlation with SiO_2, while Na_2O and K_2O increase as SiO_2 increases, and they exhibit a positive correlation with SiO_2. The Harker diagrams of the Major elements have linear and near-linear trends, suggesting that the acid-to-acid-to-basic dike may be comagmatic. Higher contents of MgO, TiO_2, CaO, and Fe oxides and low contents of K_2O and Na_2O in

basic rocks relative to acidic rocks are known as normal trends. These variation diagrams indicate a normal fractional crystallization in magma. Some samples are scattered on the Harker diagrams, probably due to alteration and some systematic errors.

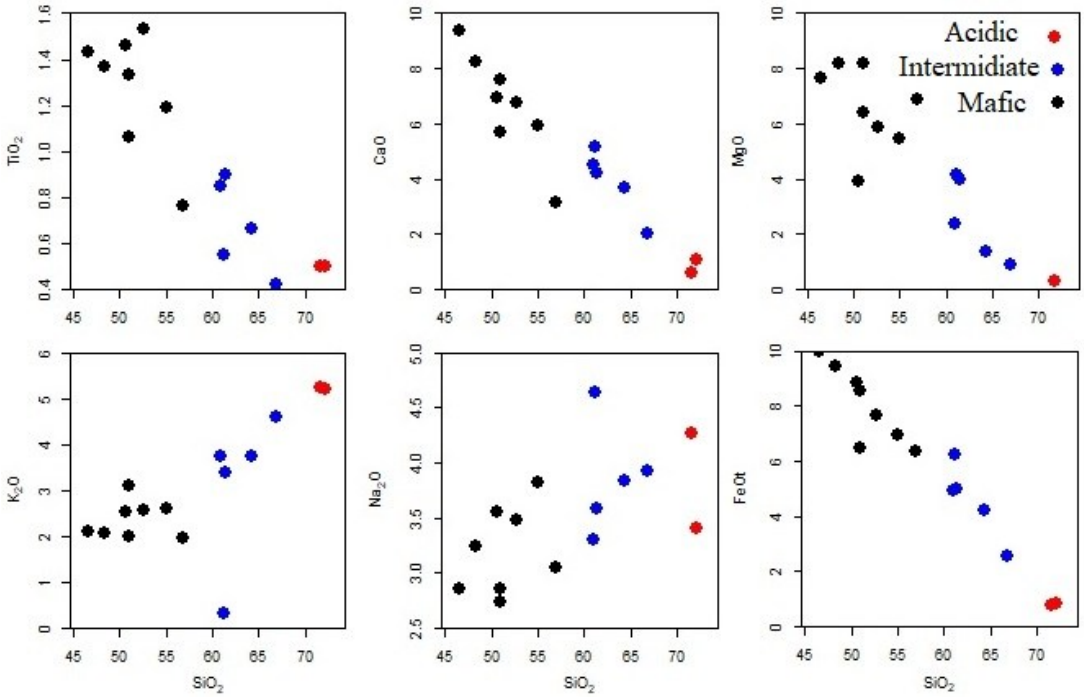

Fig. 7. Selected Harker variation diagrams of major elements (wt. %) vs. SiO_2 (wt. %) for the Siahjakuk dikes.

5.3. Minor elements

As the SiO_2 increases, the Ni, Ce, Cr, La, Y, Zr, and Sr decrease while Rb increases (Fig. 8). The trends are mainly linear or near linear, which may suggest the co-genetic nature of all dikes.

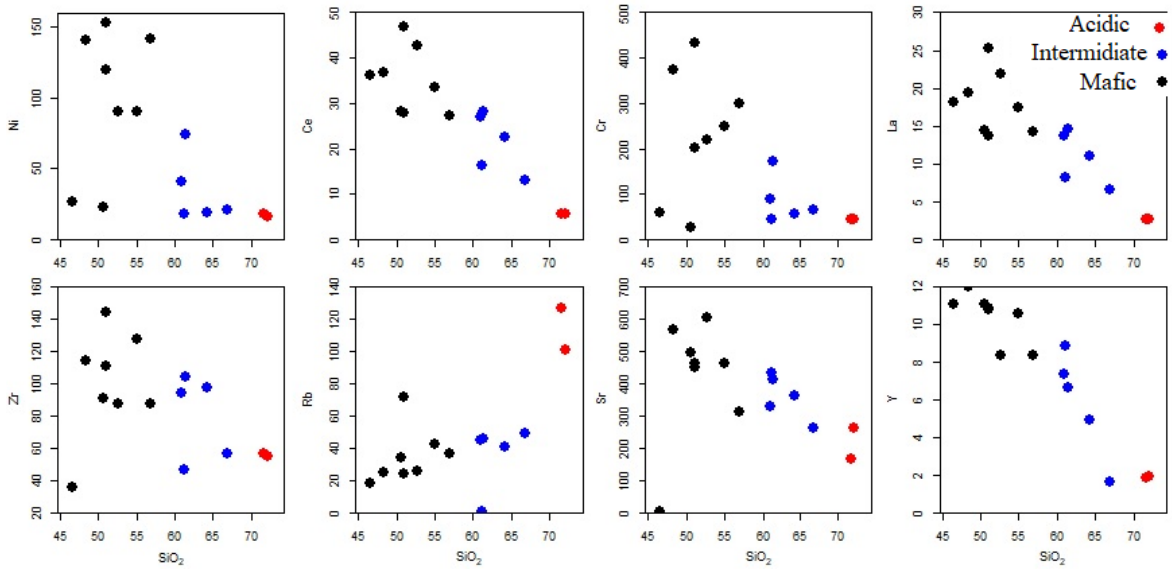

Fig. 8. Selected Harker variation diagrams of minor elements (wt. %) vs. SiO_2 (wt. %) for the Siahjakuk dikes.

5.4. Magmatic series

According to TAS diagram [23], as shown in Figure 6, the dikes are sub-alkaline and alkaline in the magmatic series. In this diagram, the basic dikes are mainly alkaline and the intermediate and acidic dikes are mainly subalkaline (Fig. 6A). According to SiO_2-K_2O diagram of Peccerillo and Taylor [24], the chemical composition of the dikes is similar to high K calc-alkaline and shoshonitic magmatic rocks (Fig. 9A). The Th/Yb-Ta-Yb diagram divides those rocks that are calc-alkaline from those that are shoshonitic. This diagram shows that the study dikes are mainly shoshonitic (Fig. 9B).

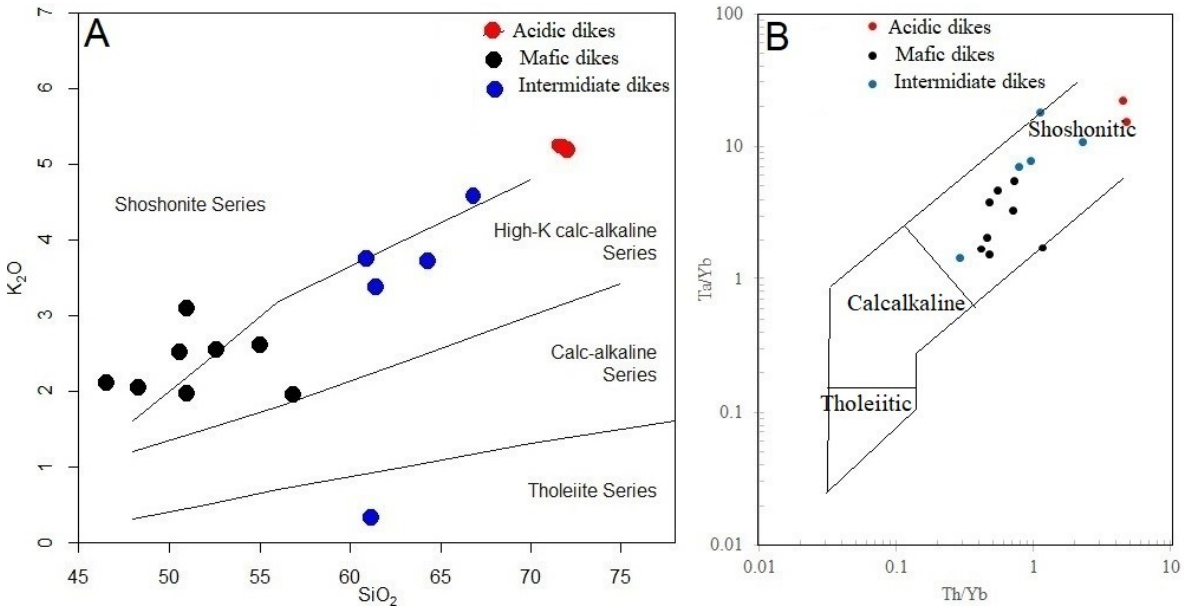

Fig. 9.(A) Distribution of the dikes in SiO_2 vs. K_2O of Peccerillo and Taylor, [24], (B) Distribution of the di kes in Th/Yb vs. Ta/Yb of Muller [25].

5.5. Tectonic setting

The high K calk-alkaline and shoshonitic rocks occur in several tectonic settings, such as initial and late oceanic arcs, continental arcs, collisional, post-collisional rocks, and within-plate [25, 26]. According to Nb/Yb- Th-Yb of Pearce [27], the dikes are related to a volcanic arc (Fig. 10A). Figure 10B shows that the composition of the dikes mainly falls in the island arc field [28] while in some diagrams they plot in the continental margin field. According to ternary diagram of Wood [29], they are mainly similar to continental arc basalts in composition (Figure 10C). Fig 10D discriminates potassic rocks that form in volcanic arc plates (VAP) and within plates (WIP). This diagram shows the study sample plots in VAP field. Figure 10E which discriminates between continental arc plates (CAP) and post-collisional plates (PAP), indicates that the study dikes are post-collisional (PAP).

The rifting, subduction, collision and post-collisional events, respectively, (a complete orogenic cycle) in the SSZ from Cretaceous (similar to other parts of Iran) were confirmed by the majority of researchers. The mechanism and timing of the opening and closing of the ocean basin have been debated by a few researchers [1, 30, 31, 32, 33]. The timing of the collision of the Lut and Afghan blocks is Late Cretaceous [30] or Middle Eocene [1], while the study dikes are Oligo-Miocene in age. Therefore, the dikes are at least younger than the subduction event in the SSZ. With regard to the age and the geochemical data, the dikes are probably related to post-collision magmatism.

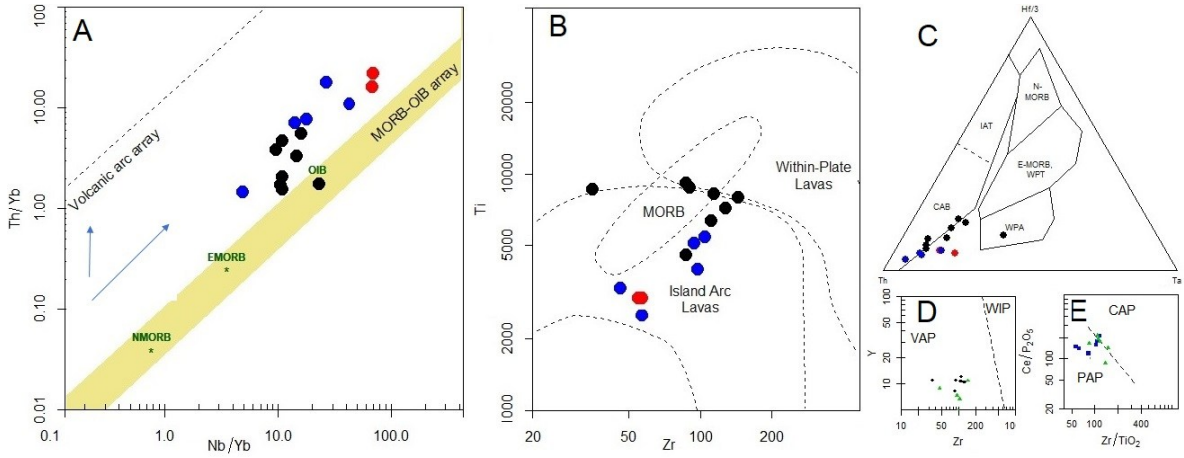

Fig.10. Plot of the Siahjakuk dikes compositions in tectonic discrimination diagrams. (A) Nb/Yb vs. Th/Yb. (B) Zr vs. Ti. (C) Ta-Ta-Hf/3. (D) Zr vs. Y. (E) Zr/TiO2 vs. Ce/P_2O_5 for potassic igneous rocks with location of the LIC igneous rocks. IOP: Initial oceanic arc, LOP: Late oceanic arc, CAP: Continental arc, PAP: Post-collisional arc.

5.6. Spider diagrams

Chondrite-normalized REE plots [34] of dykes show that the rocks are more enriched in LREE relative to HREE (Fig. 11A, B and C). The REE pattern of basic to acidic dikes shows a deep (LREE) to intermediate (HREE) slope with weak negative Eu anomalies (except one sample that has no Eu anomaly) (Figure 11A and B). Weak negative anomalies indicate minor plagioclase fractionation [35]. The REE pattern of the basic, intermediate, and acidic rocks is almost similar, and all samples have a parallel and sub-parallel pattern (Fig. 11, A, B, C) that indicates they had probably derived from the same origin and in a similar way. The acidic dikes are also characterized by a weak negative Dy anomaly that may be due to analytical error, as their values are near to sensitivity limit (Fig. 11C). Generally, the total REE contents decrease from basic dikes toward acidic dikes. This means that as the SiO_2 decreases, the total contents of REE increase. Primitive-normalized spider [36] plots of dikes show that the study dikes are more enriched in LILE relative to HFSE (11 D, E, F). These diagrams show that most dikes are characterized by sharp positive K and Pb anomaly and positive Ba, Sr, Zr, and Ti anomaly. The positive Ti anomaly is also weak for most samples.

6. Discussion

According to Muller et al [25], the PAP is the most complex case of subduction-related magmatism in suture zones. In this setting, the crustal thickening is characterized by complex magmatic activity and tectonic uplift [26] and includes shoshonitic and K-rich rocks and lamprophyres [37, 38, 39]. After a collision, potassic igneous rocks may be emplaced as dikes, which are often followed by alkaline volcanism when extensional tectonic regimes develop as a consequence of uplift [26; 25]. K-rich magmas in a post-collisional tectonic setting are usually derived by partial melting of heterogeneous, enriched mantle sources that have been metasomatically enriched in LILE and LREE related to HFSE and HREE, respectively [40, 41, 42, 43, 44, 45, 46, 47].

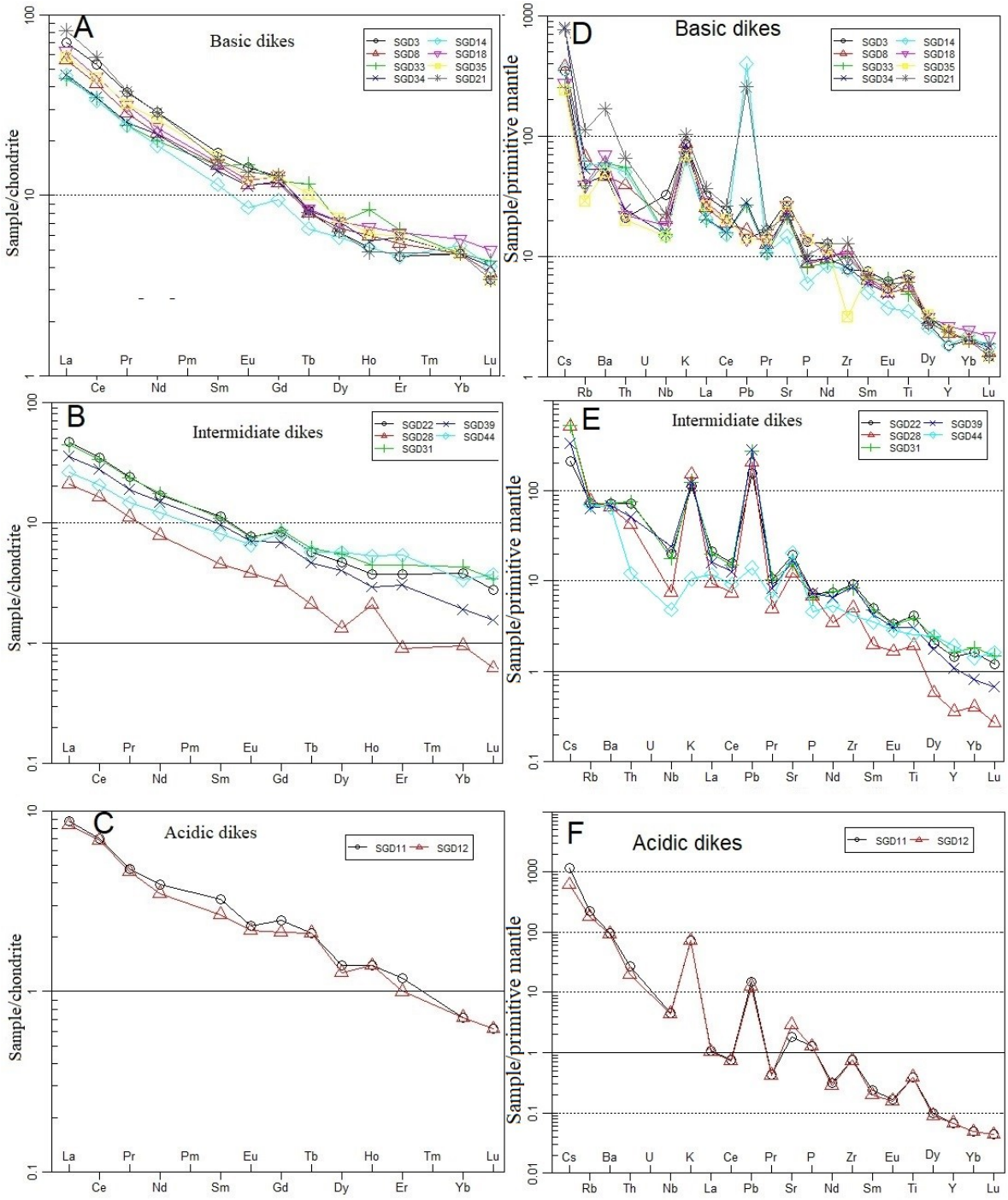

Fig. 11. (A, B, C) Chondrite-normalized REE patterns [34] of the Siahjakuk dikes. (B, C, D) Primitive mantle normalized spider diagrams [36] of the Siahjakuk dikes.

The composition of the study dikes shows that they mainly were formed from magma that was generated by the partial melting of mixed asthenosphere and lithosphere (Fig. 12A) [48]. Rocks related to an enriched source have Zr/Y ratio of more than 2.46 [33]. The study dikes have an Zr/Y of >3.22, which is in accordance with an enriched source (Fig. 12B) [49]. The composition of the dikes in Fig. 12C shows that

both sediment melts and slab-derived fluids had some role in the magma generation [50]. The higher enrichment of LREE and LILE relative to HREE and HFSE, respectively, is usually reported to be a characteristic of subduction zones that were likely inherited from a mantle source that had been metasomatized by melts/fluids released from a subducting slab, or modified by subducted sediments and associated fluids/melts [51, 52, 53].

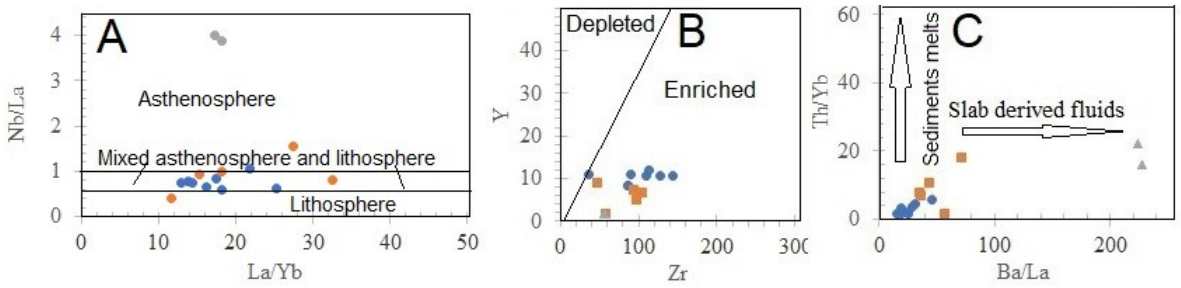

Fig. 12. (A) Plot of the dikes in La/ Yb vs. Nb/ La diagram of Abdel-Fattah and Philip [48]. (B) Diagram of Zr vs. Y of Abu-Hamatteh [49] showing the enriched nature of the dikes. (C) Ba/La vs. Th/Yb diagram of Shaw [49] showing the dikes follow a trend between slab-derived fluids and sediment melt arrays.

Ni, Cr, and SiO_2 contents in primary mafic magma are 1400 to 1500 ppm, <1000 ppm, and <50%, respectively [54]. Ni, Cr, and SiO_2 in the study dikes range from 27 to 153 ppm, 28 to 432 ppm, and 46 to 73 wt. %, respectively, especially the acidic and intermediate dikes that have very low contents of Ni and Cr, and Mg (Table 1), indicating they were not directly formed from a primary mantle magma. Such magmas may be generated from primary mafic magma by AFC and FC or generated by partial melting of different sources. The low concentration of Ni, and Cr also could be due to early fractionation of olivine or clinopyroxene [55]. The felsic dikes with low Ti, may have mainly resulted from fractionation of Ti and Fe oxides. However, the basic dikes have higher TiO_2 and Mg, which may be due to the presence of Ti and Fe oxides and the presence of amphibole. Mg character of the mafic dikes in the study area is partly due to the presence of secondary chlorite. The negative correlation between SiO_2 and MgO, FeO, CaO in the study dikes may have mainly resulted from the fractionation of olivine, enstatite, diopside, and spinel [56, 57, 58, 59, 60, 61, 62, 63, 64, 65].

High contents of K_2O in the study rocks require a potassic phase such as K-F, phlogopite, and K-amphibole in the source. Weak or absence of the Eu anomaly may show that the source rocks had little feldspar, especially plagioclase. Furman and Graham [67] indicated that melts produced from phlogopite have Rb/Sr>0.1 and Ba/Rb<15, while those formed from an amphibole-bearing source have Rb/Sr< 0.06 and Ba/Rb>15. Rb/Sr ratios of the basic and acidic dikes are mainly less than 0.06, which is in accordance with an amphibole-bearing source. The Rb/Sr of the intermediate dikes is more than 0.1, which is in accordance with a phlogopite source. The Ba/Rb in the dikes (except 4 samples from mafic dikes) are mainly less than 15, indicating their magma was formed from a phlogopite-bearing source (Fig. 13A).
According to Fig. 13 B and C the mafic and intermediate dikes were formed from melts derived from partial melting of mafic rocks such as basalt and amphibolite. The basic and intermediate dikes in the amphibolite field are separated from each other, showing that their source rocks have some differences. In contrast, the acidic dikes are related to melts that derive from partial melting of crust sediments such as greywacke (Fig. 13B and C).

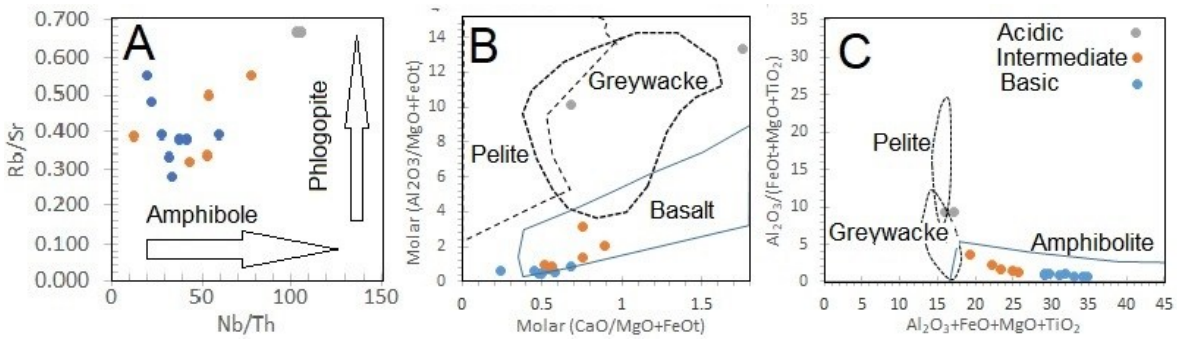

Fig. 13. (A) Diagram of Nb/Th vs. Rb/Rb of Furman and Graham [65] shows the dike compositions compared with the amphibole and phlogopite array in the magma source. (B) Molar CaO/(MgO + FeOt) vs. Molar Al2O3/(MgO + FeOt) of Althert et al. [66] showing the basic and intermediate dikes plot in the basalts field, while acidic dikes plot in the greywacke field. (C) Diagram of (Al_2O_3+FeO+MgO+TiO_2 vs. Al_2O_3/(FeO+MgO+TiO_2) of Whelen et al. [67] showing the basic and intermediate dikes plot in amphibolite field, while acidic dikes plot in greywacke and pelite fields.

The study dikes show strong correlations between major and minor elements on the Harker diagrams, suggesting genetic relations between them (Fig. 6). The observed variations and correlations could have resulted from variable partial melting (PM), fractional crystallization (FC), and assimilation and fractional crystallization (AFC). Modeling diagrams of compatible and incompatible elements can help to identify which processes played the main role in the evolution of the magma [68, 69]. The study dikes show more compatibility with trend PM and AFC (Fig. 14A, B and C), suggesting both PM and AFC had probably played roles in the magma evolution. Post-coolisional magmatism in the study area was probably caused by an upwelling of the asthenosphere and strike-slip faults and partial melting of the heterogeneous metasomatic enriched mantle in a slab zone.

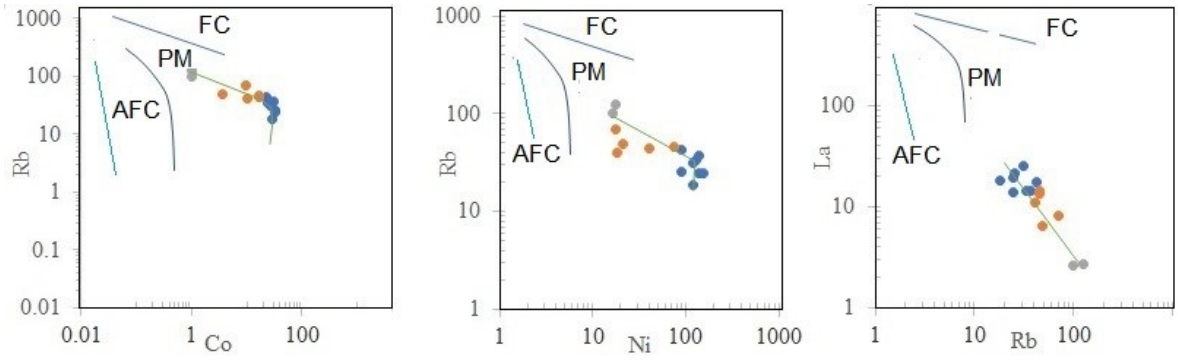

Fig. 14. Log-Log diagrams of compatible and incompatible elements.

7. Conclusion

The dikes are the youngest magmatism phase in the study area that intruded the flysch-like sedimentary rocks. The field studies show that all dikes of mafic to felsic have the same age and were mainly controlled by NW and NS faults and shear zones. The petrography studies show that the dikes had been formed under different conditions from different magmas, as they have different textures and compositions. They range from meladiorite to rhyolite in composition and can be divided into mafic, intermediate, and acidic dikes. The mafic and some intermediate dikes have granule texture and have formed in one stage, while acidic dikes and some intermediate dikes have porphyritic texture, indicating that had formed in two stages.

The dikes are characterized by arc-like geochemical affinity with enrichment of LILE and LREE relative to HFSE and HREE. They are mainly shoshonitic and high-K calc-alkaline in magmatic series and relate

to convergent plates. The dikes' age is in accordance with post-collisional events and movements of the strike-slip faults in eastern Iran following the convergence and collision of Lut and Afghan blocks.
There are at least two magmas. Neither of the magmas was not primary magma. The mafic and intermediate dikes had formed from magma that derived from the partial melting of an enriched metasomatized lithospheric mantle and had evolved by AFC. The acidic dikes are related to magma that had derived from partial melting of crustal materials. The lithospheric mantle-derived magma provided enough heat for the partial melting of crust to produce the acidic melts.
The heat, for the melting of metasomatized lithospheric mantle, was probably supplied by the upwelling of the hot asthenosphere.

Acknowledgments

We would like to pass our thanks to the University of Sistan and Baluchestan and the Iranian Mines and Mining Industries Development and Renovation Organization (IMIDRO), which provided a part of the funding for this research.

Ethical Considerations

The authors avoided data fabrication, falsification, and plagiarism, and any form of misconduct.

Funding

This research did not receive any specific grant from funding agencies in the public, commercial, or not-for-profit sectors.

Conflict of Interest

The authors declare that they have no known competing financial interests or personal relationships that could have appeared to influence the work reported in this paper.

References

[1] Camp, V.E. and Griffis, R. J. (1982). Character, genesis and tectonic setting of igneous rocks in the Sistan suture zone, eastern Iran. Lithos 15: 221-239.
[2] Tirrul, R., Bell, L.R., Griffis, R.J., Camp, V.E. (1983). The Sistan suture zone of eastern Iran. Geological Society of America Bulletin 94: 134-150.
[3] Sadeghian, M. (2005) Magmatism, metallogeny and emplacement mechanisms of Zahedan granitoidic pluton. PhD thesis, University of Tehran, Tehran (in Persian).
[4] Nazari, M., Boomeri, M., Biabangard, H., & Nakashima, K. (2022). K-and Na-rich volcanic rocks of Asagi igneous complex, eastern Iran. Arabian Journal of Geosciences, 15(11), 1025. https://doi.org/10.1007/s12517-022-10173-8
[5] Ghasemi, H., Sadeghian, M., Kord, M. and Khanalizadeh, A. (2010). The evolution mechanisms of Zahedan granitoidic batholith, southeast Iran. Iranian Journal of Crystallography and Mineralogy 17: 551-578 (in Persian).
[6] Moradi, R., Boomeri, M., Bagheri, S. (2014). Petrography and geochemistry of intrusive rocks in the Shurchah antimony-bearing area southeast of Zahedan. Petrology (Isfahan Univ.) 5: 15–32.
[7] Mohammadi, A., Burg, J.P., Bouilhol, P., Ruh, J. (2016). U-Pb geochronology and geochemistry of Zahedan and Shah Kuh plutons, southeast Iran: implication for closure of the south Sistan suture zone. Lithos 248–251: 293–308. © 2016 Elsevier B.V. https://doi.org/10.1016/j.lithos.2016.02.003
[8] Boomeri, M., Moradi, R., Stein, H., Bagheri, S. (2019). Geology, Re-Os age, S and O isotopic composition of the Lar porphyry Cu-Mo deposit, southeast Iran. *Ore Geology Reviews*, 104: 477–494. https://doi.org/10.1016/j.oregeorev.2018.11.018

[9] Boomeri, M., Moradi, R., Bagheri, S. (2020). Petrology and origin of the Lar igneous complex of the Sistan suture zone, Iran. *Geologos,* 26: 51–64. https://doi.org/10.2478/logos-2020-0004
[10] Stöcklin, J. (1968). Structural history and tectonics of Iran, a review. *American Association of Petroleum Geologists Bulletin*, 52, 1229-1258. https://doi.org/10.1306/5D25C4A5-16C1-11D7-8645000102C1865D
[11] Mokhtari, Z., Boomeri, M., Bagheri, S. (2015). Digital image processing and analysis techniques for detection of hydrothermal alteration zones: A case study in Siah-Jangal Area, north of Taftan Volcano, southeastern Iran. *Journal of Indian Society of Remote Sensing*, 43(3): 363–377. https://doi.org/10.1007/s12524-014-0422-4
[12] Mokhtari, Z., Boomeri, M. and Bagheri, S. (2015). Application of multifractal modeling technique in systematic lithogeochemical survey to identify Au–Cu anomalies in the Siah-Jangal area, Southeastern of Iran. *Arabian Journal Geoscience*, 8 (1): 9517–9530. https://doi.org/10.1007/s12517-015-1860
[13] Moradi, R., Boomeri M. (2016). Remote sensing detection of altered zones associated with Cu-Mo mineralization in north of Zahedan, SE Iran using Landsat-8 data. *Yerbilimleri*, 38: 275–294.
[14] Moradi, R., Boomeri, M., Bagheri, S., Nakashima, K. (2016). Mineral chemistry of igneous rocks in the Lar Cu-Mo prospect, southeastern part of Iran: Implications for P, T, and fO_2. *Türkish Journal of Earth Sciences*, 25, 1–16. https://doi.org/10.3906/yer-1510-5
[15] Hedayati, N., Boomeri, M., Biabangard, H. (2016). Petrography and geochemical characteristics of Nakhilab igneous complex, northwest of Zahedan. Petrology 27: 23–44, (in Persian with English abstract). https://doi.org/10.22067/econg.2022.69941.1017
[16] Ghodsi, M.R., Boomeri, M., Bagheri. S., Ishiyama, D., Corfu, F. (2016). Geochemistry, zircon U-Pb age, and tectonic constraints on the Bazman granitoid complex, southeast Iran. *Turkish Journal of Earth Science*, 25(4): 311–340. https://doi.org/10.3906/yer-1509-3
[17] Bagheri, S., Damani Gol, Sh. (2020) The eastern Iranin orcline, *Earth-Science Reviews*, 210, https://doi.org/10.1016/j.earscirev.2020.103322
[19] Berberian, M. (1983). Geological map of Zahedan qudrangle 1/100000, Geological Survey of Iran.
[20] Rezaei-Kahkhaei, M., Rahbar, R., Ghasemei, H., (2017). Dating of Lakhshak intrusive assemblage through the U-Pb method on zircon and titanite, East Iran. *The Iranian Journal of Crystallography and Mineralogy*, 25(1): 111-122.
[21] Whitney, D.L., Evans, B.W. (2010). Abbreviation for names of rock forming minerals. *American Mineralogist*, 95(1): 185-187. https://doi.org/ 10.2138/am.2010.3371
[22] Cox, K.G., Bell, J.D., Pankhurst, R.J. (1979). The interpretation of igneous rocks, George Allen and Unwin, London.
[23] Harker, A. (1909). The Natural History of Igneous Rock. Macmillan, New York, 384.
[24] Pecerillo, A., Taylor, S.R. (1976). Geochemistry of Eocene calc-alkaline volcanic rocks from the Kastamonu area, northern Turkey, Contributions to Mineralogy and Petrology 58: 63–81. https://doi.org/10.1007/BF00384745
[25] Müller, D., Rock, N.M.S, Groves, D.I. (1992). Geochemical discrimination between shoshonitic and potassic volcanic rocks from different tectonic settings: a pilot study. *Mineralogy and Petrology*, 46(4): 259-289. https://doi.org/10.1007/BF01173568
[26] Wilson, M. (1989) Igneous petrogenesis, A global tectonic approach. Unwin Hyman London: 466.
[27] Pearce, J.A. (2008). Geochemical fingerprinting of oceanic basalts with applications to ophiolite classification and the search for Archean oceanic crust. *Lithos*, 100(1-4), 14-48. https://doi.org/10.1016/j.lithos.2007.06.016
[28] Pearce, J.A. (1982). Trace element characteristics of Lavas from destructive plate boundaries. In: Thorpe RS (Ed) Andesites Wiley, New York: 525-548.
[29] Wood, D.A. (1980) The Application of a Th-Hf-Ta diagram to problems of tectonomagmatic classification and to establishing the nature of crustal contamination of basaltic lavas of the British tertiary volcanic province. *Earth and Planetary Science Letters*, 50(1): 11-30.

https://doi.org/10.1016/0012-821X(80)90116-8
[30] Zarrinkoub, M.H., Pang, K.N., Chung, S.L., Khatib, M.M., Mohammadi, S.S., Chiu, H.Y., Lee, H.Y. (2012). Zircon U–Pb age and geochemical constraints on the origin of the Birjand ophiolite, Sistan suture zone, eastern Iran. *Lithos*, 154: 392-405. https://doi.org/10.1016/j.lithos.2012.08.007
[31] Pang, K.N., Chung, S.L., Zarrinkoub, M.H., Khatib. M.M., Mohammadi, S.S., Chiu, H.Y., Chu, C.H., Lee, H.Y., Lo, C.H. (2013). Eocene-Oligocene post-collisional magmatism in the Lut-Sistan region, eastern Iran: magma genesis and tectonic implications. *Lithos*, 180-181: 234-251. https://doi.org/ 10.1016/j.lithos.2013.05.009
[32] Arjmandzadeh, R., Karimpour, M.H., Mazaheri, S.A., Santos, J.F., Medina, J.M., Homam, S.M. (2011). Two-sided asymmetric subduction: implications for tectonomagmatic and metallogenic evolution of the Lut Block, eastern Iran. *Journal of Economic Geology*, 3: 1-14. https://doi.org/ 10.22067/econg.v3i1.11445
[33] Saccani, E., Delavari, M., Beccaluva, L., Amini, S.A. (2010). Petrological and geochemical constraints on the origin of the Nehbandan ophiolitic complex (eastern Iran): Implication for the evolution of the Sistan Ocean. *Lithos*, 117(1-4): 209-228. https://doi.org/https://doi.org/10.1016/j.lithos.2010.02.016
[34] Nakamura, N. (1974). Determination of REE, Ba, Fe, Mg, Na and K in carbonaceous and ordinary chondrites. *Geochimica et Cosmochimica Acta*, 38: 757-775. https://doi.org/ https://doi.org/10.1016/0016-7037(74)90149-5
[35] Rollinson, H. R. (1993) Using geochemical data: Evolution, Presentation, interpretation. Longman, Singapore, 353.
[36] Sun, S., McDonough, W.F. (1989). Chemical and isotopic systematics of oceanic basalts: Implications for mantle composition and processes. *Geological Society London, Special Publications,* 42(1): 313–345. https://doi.org/10.1144/GSL.SP.1989.042.01.19
[37] Bonin, B.L., Azzouni-Sekkal, A., Bussy, F., Ferrag, S. (1998). Alkali-calcic and alkaline post-orogenic (PO) granite magmatism: petrologic constraints and geodynamic settings. *Lithos,* 45(1): 45-70. https://doi.org/10.1016/S0024-4937(98)00025-5
[38] Vaughan, A.P.M., Sacrow, J.M. (2003). K-rich mantle metasomatism control of localization and initiation of lithospheric strike-slip faulting. *Terra Nova,* 15: 163-169. https://doi.org/ https://doi.org/10.1046/j.1365-3121.2003.00485.x
[39] Seifert, T.h. (2008). Metallogeny and Petrogenesis of Lamprophyres in the Mid-European Variscides. Amsterdam, 303p.
[40] Edgar, A.D. (1987). The genesis of alkaline magmas with emphasis on their source regions: inferences from experimental studies. In: Fitton. J.G., Upton, B.G.J. (Eds), Alkaline Igneous Rocks. *Geological Society Special Publication*, 30: 29-52. https://doi.org/https://doi.org/10.1144/GSL.SP.1987.030.01.04
[41] Foley. S.F., Peccerillo, A. (1992). Potassic and ultrapotassic magmas and their origin. *Lithos*, 28(3-6): 181-185. https://doi.org/https://doi.org/10.1016/0024-4937(92)90005-J
[42] Guo, Z., Wilson, M., Zhang, M., Cheng, Z., Zhang, L. (2013). Post-collisional, K-rich mafic magmatism in south Tibet: constraints on Indian slab-to-wedge transport processes and plateau uplift. *Contributions to mineralogy and petrology*, 165(6): 1311-1340. https://doi.org/10.1007/s00410-013-0860-y
[43] Kuritani, T., Kimura, J., Ohtani, E., Miyamoto, H., Furuyama, K. (2013). Transition zone origin of potassic basalts from Wudalianchi Volcano, northeast China. *Lithos*, 156-159: 1-12. https://doi.org/10.1016/j.lithos.2012.10.010
[44] Tan, J., Wei, J.H., Shi, W.J., Feng, B., Li, Y.J., Fu, L.B. (2013). Origin of dyke swarms by mixing of metasomatized subcontinental lithospheric mantle-derived and lower crustal magmas in the Guocheng fault belt, Jiaodong Peninsula, North China Craton. *Geological Journal*, 48: 516-530. https://doi.org/10.1002/gj.2472
[45] Bucholz, C.E., Jagoutz, O., Schmidt, M.W., Sambuu, O. (2014). Fractional crystallization of high-K arc magmas: biotite- versus amphibole-dominated fractionation series in the Dariv Igneous Complex, western Mongolia. *Contributions to Mineralogy and Petrology*, 168(5): 1072-1100.

https://doi.org/ 10.1007/s00410-014-1072-9
[46] Aghazadeh, M., Prelevic, D., Badrzadeh, Z., Braschi, E., van den Bogaard, P., Conticelli, S. (2015). Geochemistry Sr–Nd–Pb isotopes and geochronology of amphibole and mica-bearing lamprophyres in northwestern Iran: implications for mantle wedge heterogeneity in a paleo-subduction zone. *Lithos,* 217: 352-369. https://doi.org/10.1016/j.lithos.2015.01.001
[47] Yang, Z.M., Lu, Y.J., Hou, Z.Q., Chang, Z.S. (2015). High-Mg diorite from Qulong in southern Tibet: implications for the genesis of adakite-like intrusions and associated porphyry Cu deposits in collisional orogens. *Journal of Petrology*, 56(2): 227-254. https://doi.org/10.1093/petrology/egu076
[48] Abdel- Fattah, M., Philip, E.N. (2004). Cenozoic Volcanism in the Middle East: Petrogenesis of Alkali Basalts from Northern Lebanon, *Geological Magazine*, 141(5): 545-563. https://doi.org/10.1017/S0016756804009604
[49] Abu- Hamatteh, Z.S.H. (2005). Geochemistry and Petrogenesis of Mafic Magmatic Rocks of the Jharol Belt, India: Geodynamic Implication, *Journal of Asian Earth Science,* 25(4): 557-581. https://doi.org/10.1016/j.jseaes.2004.05.006
[50] Shaw, DM. (1970) Trace element fractionation during anatexis. *Geochimica Cosmochimica Acta*, 34: 237‑243. https://doi.org/10.1016/0016-7037(70)90009-8
[51] Foley, S.F., Venturelli, G., Green, D.H., Toscani. L. (1987). The ultrapotassic rocks: characteristics, classification, and constraints for petrogenetic models. *Earth- Science Review*, 24(2): 81-134. https://doi.org/10.1016/0012-8252(87)90001-8
[52] Altherr, R., Holl, A., Hegner, E., Langer, C., Kreuzer, H.. (2002). High potassium, calc-alkaline I-type plutonism in the European Variscides northern Vosges (France) and northern Schwarzwald (Germany). *Lithos,* 50(1): 51-73. 10.1016/S0024-4937(99)00052-3
[53] Boari, E., Tommasini, S., Laurenzi, M.A., Conticelli, S. (2009). Transition from ultrapotassic kamafugitic to sub-alkaline magmas: Sr, Nd, and Pb isotope, trace element and Ar^{40}-Ar^{39} age data from the middle Latin valley volcanic field, Roman magmatic province, central Italy. *Journal of Petrology*, 50(7): 1327-1357. https://doi.org/10.1093/petrology/egp003
[54] Glenn, A.G. (2004). The influence of melt structure on trace element partitioning near the Peridotite solidus. *Contributions to Mineralogy and Petrology*, 147, 511-527. https://doi.org/10.1007/s00410-004-0575-1
[55] Woodard, J., Kietäväinen, R., Eklund, O. (2014). Svecofennian post-collisional shoshonitic lamprophyres at the margin of the Karelia Craton: Implications for mantle metasomatism. *Lithos,* 205, 379-393. https://doi.org/10.1016/j.lithos.2014.06.021
[56] Mason, B., Moor, C.B. (1982). Principle of geochemistry, 4th ed. John Wiley and Sons, New York, 344.
[57] Norman, MD., Leeeman, W.P. (1989). Open system magmatic evolution of andesites and basalts from the Salmon Greek-volcanic, south western Idaho. U.S.A. *Chemical Geology*, 81(3): 167-189. https://doi.org/10.1016/0009-2541(90)90114-M
[58] Leeman, W.P., Smith, D.R., Hildreth, W., Palacz Rogers, N. (1990). Compositional diversity of late Cenozoic basalts in a transect across the southern Washington Cascades: implications for subduction zone magmatism. *Journal of Geophysical Research*, 95(B12), 19561-19582. https://doi.org/10.1029/JB095iB12p19561
[59] Pearce, J.A., David, W. (1991). The role of carbon taxes in adjusting to global warming. *Economic Journal, Royal Economic Society*, 101(7), 938-948. https://doi.org/10.2307/2233865
[60] Calanchi, N., Peccerillo, A., Tranne, C.A., Lucchini, F., Rossi, P.L., Kempton, P., Barbieri, M., Wue, T.W. (2002). Petrology and geochemistry of volcanic rocks from the island of Panarea: implications for mantle evolution beneath the Aeolian Island arc (southern Tyrrhenian sea). *Journal of Volcanology and Geothermal Research*,115(3-4): 367-395. https://doi.org/10.1016/S0377-0273(01)00333-X
[61] Karen, R., Thomas, A., Thomas, W. (2002). Origin and emplacement of the andesite of Burroughs Mountain, a zoned, large volume lava flow at Mount Rainier, Washington, USA. *Journal of Volcanology and Geothermal Research*, 119(1-4): 275-296. https://doi.org/10.1016/S0377-0273(02)00358-X

[62] Cook, C., Briggs, R.M., Smith, I.E.M., Mass, R. (2005). Petrology and geochemistry of intraplate basalts in the south Aulis and volcanic field, New Zealand: evidence for two coeval magma suites from distinct sources. *Journal of Petrology*, 46(3), 473-503. https://doi.org/10.1093/petrology/egh084

[63] Aragon, E., Gonzalez, P., Yolanda, E., Cavarozzi, A.C., Liambias, E., Rivalenti, G. (2002). Thermal divide andesites-trachytes, petrologic evidence and implications from Jurassic north Patagonian massif alkaline volcanism. *Journal of South American Earth Sciences,* 16(3):91-103. https://doi.org/10.1016/S0895-9811(03)00046-4

[64] Ali, S.A. (2012). Geochemistry and geochronology of Tethyan-arc related igneous rocks, NE Iraq. Ph.D. thesis, University of Wollongong, 363.

[65] Furman, T., Graham, D. (1999). Erosion of lithospheric mantle beneath the East African Rift system: geochemical evidence from the Kilvu volcanic province. *Lithos*, 48(1-4): 237-262. https://doi.org/10.1016/S0024-4937(99)00031-6

[66] Altherr, R., Topuz, G., Siebel, W., Sen, C., Meyer, H.P., Satir, M., Lahaye, Y. (2008). Geochemical and Sr–Nd–Pb isotopic characteristics of Paleocene plagioleucitites from the Eastern Pontides (NE Turkey). *Lithos*, 105(1): 149-161. https://doi.org/10.1016/j.lithos.2008.03.001

[67] Whalen, J.B. and Currie, K.L.B.W. (1987) A-type granite: geochemical characteristics, discrimination and petrogenesis. *Contibutions to Mineralogy and Petrology,* 95(4): 407-419. https://doi.org/10.1007/BF00402202

[68] Cocherie, A.. (1986). Systematic use of trace element distribution patterns in log-log diagrams for plutonic suites. *Geochimica et Cosmochimica Acta*, 50(11): 2517-2522. https://doi.org/10.1016/0016-7037(86)90034-7

[69] Costa, S.; Masotta, M.; Gioncada, A.; Pistolesi, M. A. (2021) Crystal Mush Perspective Explains Magma Variability at La Fossa Volcano (Vulcano Island, Italy). *Minerals*, 11, 1094. https://doi.org/ 10.3390/min11101094